Recep Tayyip Erdoğan Üniversitesi Fen ve Mühendislik Bilimleri Dergisi, 6(3) 886-904 2025
Recep Tayyip Erdogan University Journal of Science and Engineering, 6(3) 886-904 2025
ISSN: 2687-2315 / E-ISSN: 2757-7686

Parametric CAD Modelling of Octahedral Lattice Structures for Vibration Reduction in Tool

EKREM ÖZKAYA [1*]

[1] Faculty of Engineering and Architecture-Department of Mechanical Engineering, Recep Tayyip Erdoğan University, Rize, Türkiye.

Sorumlu Yazar/Corresponding Author
E-mail: ekrem.ozkaya@erdogan.edu.tr

Araştırma Makalesi/Research Article
Geliş Tarihi/Received: 30.10.2025
Kabul Tarihi/Accepted: 27.11.2025

Abstract

This paper presents the development of a three-dimensional internal lattice structure for volume modelling using Computer-Aided Design (CAD), suitable for Selective Laser Melting (SLM). Based on the favorable physical and geometric characteristics of the truncated octahedron, a uniformly distributed cellular architecture was created to achieve high mechanical efficiency. For this purpose, a parametric software tool, OctMatrix, was developed to generate customizable matrix geometries derived from mathematical formulation. The aim of the study was to design a stable and dynamically optimized lightweight structure to reduce vibrations in a turning tool holder. Numerical and experimental investigations were performed on a conventional solid-steel tool holder and on three tool holders incorporating truncated-octahedral lattice structures. The results show significant improvements in dynamic behavior: total deformation was reduced by approximately 90%, and equivalent stress decreased by around 18%, demonstrating the strong vibration-damping potential of the lattice-reinforced design. By enabling automated and parameterized 3D CAD modelling, the OctMatrix approach represents a notable innovation for the tailored design of lightweight structures intended for additive manufacturing. This contributes to improved dynamic performance in machining applications and provides a foundation for future customization and optimization of lattice-based tool holder systems.

Keyworsds: Additive manufacturing, bionic 3D modell, selective laser melting, software module, truncated octahedron, vibration reduction.

Takım Tutucularda Titreşim Azaltımı için Oktahedral Kafes Yapıların Parametrik CAD Modellemesi

Öz

Bu makale, Seçici Lazer Ergitme (SLM) için uygun olan Bilgisayar Destekli Tasarım (CAD) kullanılarak hacim modelleme için üç boyutlu bir iç kafes yapısının geliştirilmesini sunmaktadır. Kesik oktahedronun elverişli fiziksel ve geometrik özelliklerine dayanarak, yüksek mekanik verimlilik elde etmek için düzgün dağılımlı bir hücresel mimari oluşturulmuştur. Bu amaçla, matematiksel bir formülasyondan türetilen özelleştirilebilir matris geometrileri oluşturmak için OctMatrix adlı parametrik bir yazılım aracı geliştirilmiştir. Çalışmanın amacı, torna takım tutucusundaki titreşimleri azaltmak için kararlı ve dinamik olarak optimize edilmiş hafif bir yapı tasarlamaktı. Geleneksel katı çelik takım tutucusu ve kesik sekiz yüzlü kafes yapıları içeren üç takım tutucusu üzerinde sayısal ve deneysel araştırmalar yapılmıştır. Sonuçlar, dinamik davranışta önemli iyileşmeler olduğunu göstermektedir: toplam deformasyon yaklaşık %90 oranında azalmış ve eşdeğer gerilme yaklaşık %18 oranında azalmıştır, bu da kafesle güçlendirilmiş tasarımın güçlü titreşim sönümleme potansiyelini göstermektedir. Otomatik ve parametreleştirilmiş 3D CAD modellemeyi mümkün kılan OctMatrix yaklaşımı, eklemeli imalat için tasarlanmış hafif yapıların özel tasarımında dikkate değer bir yenilik teşkil etmektedir. Bu, işleme uygulamalarında dinamik performansın iyileştirilmesine katkıda bulunmakta ve kafes tabanlı takım tutucu sistemlerinin gelecekteki özelleştirilmesi ve optimizasyonu için bir temel sağlamaktadır.

Anahtar Kelimeler: Biyonik 3D model, katmanlı üretim, kesik octahedron, seçici lazer eritme, titreşim azaltma yazılım modülü.

Cite as;
Özkaya, E. (2025). Parametric CAD modelling of octahedral lattice structures for vibration reduction in tool. *Recep Tayyip Erdogan University Journal of Science and Engineering,* 6(3), 886-904. Doi: 10.53501/rteufemud.1813260

1. Introduction

Vibrations are a central problem in machining, e.g. during drilling, milling and turning, as they have a negative effect on component quality and the service life of machine components and tool life. The mechanical vibrations are caused by the lack of dynamic rigidity of either the machine tool, the cutting tool and workpiece material or the tool holder (Prasad and Babu, 2017). Active vibration damping is usually achieved by actuators combined with sensors and passive vibration damping by modifying the tool holder in an additive manner by increasing the dynamic stiffness (Aggogeri et al., 2017; Akesson, 2007). It is therefore important to consider dynamic properties during the design phase and to develop methods to increase dynamic stability and therefore limit the vibration of the tool or tool holder (Astakhov and Quteiro, 2008).

1.1 Additive manufacturing

Additive manufacturing (AM) is a production process developed in the 1980s that differs significantly from conventional manufacturing methods (Sames, et al., 2016; Wong and Hernandez, 2012). Additive manufacturing is used in Rapid Prototyping, Rapid Manufacturing and Rapid Tooling (Santos et al., 2006). As shown in Figure 1, additive manufacturing technologies and methods are used in various manufacturing areas such as automotive, medical, aerospace, offshore wind turbine, offshore platform and engine construction (Bikas et al., 2016). In contrast to conventional manufacturing methods, in which workpieces are machined from a solid block, the component is built up in layers out of material provided in powder form during additive manufacturing. Different metals, plastics and composites can be used as materials (Bikas et al., 2016). Fused Deposition Modelling (FDM), Layer Object Manufacturing (LOM), Stereolithography (STL) and Selective Laser Sintering (SLS) are used for non-metallic materials, while Laser Engineered Vet Shaping (LENS), Electron Beam Melting (EBM) and Selective Laser Melting (SLM) or Direct Metal Laser Sintering (DMLS) are used for metals (Li et al., 2017). Numerous AM technologies were evaluated in previous studies (Gibson, 2014; Calignano et al., 2017).

Among the metalworking manufacturing processes, the SLM is one of the most advanced additive technologies and is very well suited for the production of complex three-dimensional geometries (Sufiiarov et al., 2017; Uhlmann et al., 2015). With a highly energetically focused laser beam, the powdery material is selectively melted and the powder particles are fused during solidification (VDI 3405).

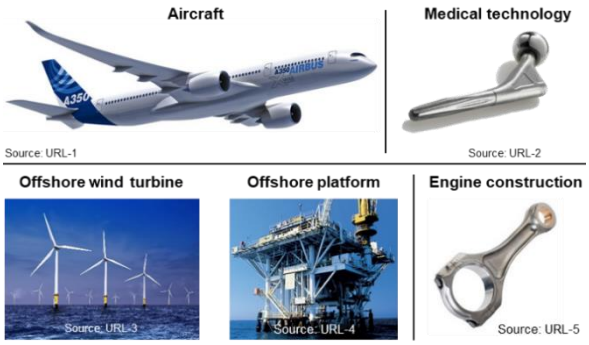

Figure 1. Application examples; Sources (URL-1, 2025; URL-2, 2024; URL-3, 2025; URL-4, 2024 URL-5, 2024)

1.2 Additive CAD support structure models

In additive manufacturing, various types of support structures such as block, point or line supports are used according to the desired properties. Typical support structures for the SLM process are lattice or honeycomb structures, which cannot be free-floating as with plastic sintering, but must always be firmly connected to the component (Cacace et al., 2017). Usually, designers are accustomed to designing components according to casting or machining principles and methods and therefore have little or no experience in the development of products for additive manufacturing (Guessasma et al., 2015). Therefore, the additive design process has to be rethought, so that developed CAD models could be optimally manufactured and the additive technology could be supported and successfully established (Vayre et al., 2012). CAD modelling data is the central source of information for data

transfer to the AM software (Mellor, et al., 2014; Vaidya and Anand, 2016). Although the additive design optimizations are repeatedly attributed revolutionary capabilities in terms of "limitless" complexity, additive manufacturing processes are mostly used for minimal requirements and when consequences for failure can be ignored or easily overcome (Jared et al., 2017). The disadvantages of the support topology between different cell types have to be overcome, including the transitions between struts, nodes and sharp edges. Subsequently, the regular graduated development of a support structure with an optimal distribution of the cell structure density according to the object weight distribution would be possible (Strano et al., 2013).

Whereas in traditional manufacturing, experimentally determined values serve as input variables and for the validation of simulation models, additive structures have to be built up using CAD models, and the component behavior is then predicted by means of simulation analyses. In order to create a complete support structure, all individual CAD models must be generated in such a way that each element can receive an input and send feedback for generations. In the field of adapted commercial design solutions, research and development still have to be carried out, so that each innovation step in this direction makes an important contribution to the significant improvement of the process (Jared et al., 2017). Particularly when creating cell structures, the number of individual CAD models is too high, so that alternative approaches are required (Robbins et al., 2016).

The upper section of Figure 2 shows the conventional process sequence of additive manufacturing. The middle and lower section visualize the modelling of the 3D support structure using the software module presented in this paper. The top row of Figure 2 schematically shows the steps of the conventional additive manufacturing process (data preparation, support structure creation, slicing, laser sintering, and post-processing steps). These steps have been added to provide reference for the additional design stages required by the newly developed OctMatrix-based modeling approach. In order to carry out the first additive process step with the new design solution integrating a truncated octahedron matrix and submitting the CAD modelling data to the AM software for the SLM process, innovation steps, which are discussed in detail in chapter 4, were necessary. With the developed software module called OctMatrix, the truncated octahedron element could be specified with selectable edge and corner diameters, and a room-filling cell matrix structure could be built up inside the tool holder.

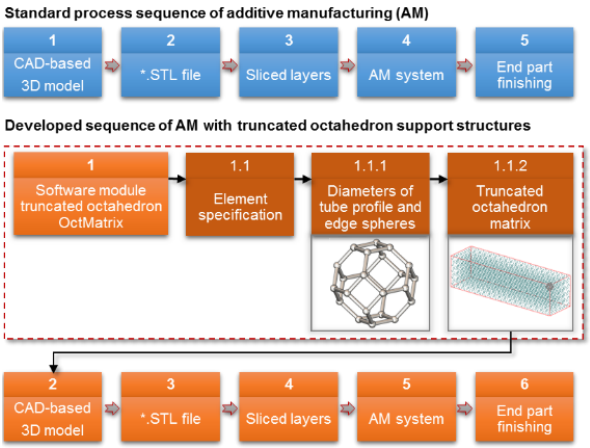

Figure 2. Process sequence of conventional additive manufacturing in comparison to the innovative process sequence for creating 3D support structures with OctMatrix

2. Theory and formulation

2.1 Methods of dynamic modelling

Many theories have been developed over the years to describe oscillations in beams on the basis of different assumptions and different phenomena (Han et al., 1999; Timoshenko, 1983; Weaver et al., 1991). The dynamic properties of simple models can be estimated with different approaches (Smirnova, 2010). The best known is probably the Euler Bernoulli beam theory, which was developed for isotropic slender beams. Since this calculation does not take shear deformations into account, this model has been extended. With the Timoshenko beam theory, the range of validity could also be extended to short bars and for static problems, by taking into account the shear and rotational inertia effects, as well as the stability

calculation (Timoshenko, 1921; Timoshenko, 1983; Timoshenko and Gere, 2012). The difference between these two theories is, that in the Euler-Bernoulli the cross-section is perpendicular to the bending line. The Timoshenko beam theory allows a rotation between the cross section and the bending line results from shear deformation, which is not included in the Euler Bernoulli theory. In the latter case, the beam is therefore stiffer (Abdarrhim, 2005). With regard to shear distortions, extensive research has been done since then to expand the areas of application, cross-sectional shapes and materials, e.g. in (Dolph, 1954; Huang, 1961; Thompson and Brougham, 2018).

The information of the modal properties, i.e. the natural frequencies and corresponding modal forms can be approximately determined with the Euler-Bernoulli calculation. The shear force *V(x, t)* under dynamic equilibrium conditions for forces acting in the *y* direction and when the boring beam oscillates transversely is calculated for dx as follows (Pettersson, 2002)

$$V(x,t) - \left(V(x,t) + \frac{\partial V(x,t)}{\partial x}dx\right) - \rho A dx \frac{\partial^2 u(x,t)}{\partial t^2} = f(x,t)dx. \quad (1)$$

Thereby, *u(x, t)* describes the beam deflection, *ρ* is the density of the tool holder material, *A* is the cross-sectional area in the *y*-*z* plane, *ρA dx* is the mass density and *f(x, t)* is the external force exerted on tool holder per unit length. The equilibrium of moments around the reference point at point *dx* at a distance *x* from the clamped end about the *z* axis results in:

$$\left(M(x,t) + \frac{\partial M(x,t)}{\partial x}dx\right) - M(x,t) - \left(V(x,t) + \frac{\partial V(x,t)}{\partial x}dx\right)dx - f(x,t)dx\frac{dx}{2} = 0. \quad (2)$$

If the bending moment on the right side is derived in Taylor's first order series and it is considered that dx^2 can be neglected as an infinitely small size of higher order, the equation results in:

$$\frac{\partial M(x,t)}{\partial x} = V(x,t). \quad (3)$$

The beam is exposed to a beam deflection according to the theory of material mechanics, resulting in the following term:

$$M(x,t) = EI(x)\frac{\partial^2 u(x,t)}{\partial x^2}. \quad (4)$$

Hereby, *EI(x)* is the bending stiffness, which is dependent on the material-specific modulus of elasticity and the axial moment of inertia *I(x)*. If no external force acts on the boring beam, then *f(x, t)* = 0. When equations 3 and 4 are inserted into equation 1, the free oscillation is given with:

$$\frac{\partial^2 u(x,t)}{\partial t^2} + \frac{EI}{\rho A}\frac{\partial^4 u(x,t)}{\partial x^4} = 0. \quad (5)$$

In order to solve the spatial part of equation 5, the boundary conditions of a clamped free beam must be defined, which requires four equations. The boundary conditions at the stressed end of the beam are described with equations 6 and 7, where the deflection and slope of the boring beam result in ($x = 0,\ u(x,t)|_{x=0} = 0$:

$$u(x,t)|_{x=0} = 0, \quad (6)$$

$$\frac{\partial u(x,t)}{\partial x}|_{x=0} = 0. \quad (7)$$

Subsequently, equations 8 and 9 describe the boundary conditions at the free end (*x* = l, *u(x, t)* $|_{x=l}$, where there is no bending moment and no shear force:

$$EI(x)\frac{\partial^2 u(x,t)}{\partial x^2}|_{x=l} = 0, \quad (8)$$

$$\frac{\partial}{\partial x}\left(EI(x)\frac{\partial^2 u(x,t)}{\partial x^2}\right)|_{x=l} = 0. \quad (9)$$

The vibration occurs in the *x*-*z* plane regardless of the *y* coordinate. The function *u (x, t)* describes the oscillation by specifying the deflection in z direction as a function of location *x* and time *t*. If the temporal and spatial deflection is considered in equation 5, the result is:

$$\frac{\partial^2 u(x)u(t)}{\partial t^2} + \frac{EI\partial^4}{\rho A}\frac{u(x)u(t)}{\partial x^4} = 0 \Longrightarrow \frac{\partial^2 u(t)}{\partial t^2}\frac{1}{u(t)} + \frac{EI}{\rho A}\frac{\partial^4 u(x)}{\partial x^4}\frac{1}{u(x)} = 0. \quad (10)$$

Natural or resonance frequencies of a beam, which are dependent on the temporal deflection *u(t)*, are given by:

$$u(t) = Asin(2\pi f_r t) + Bcos(2\pi f_r t) \Longrightarrow \frac{\partial^2 u(t)}{\partial t^2}\frac{1}{u(t)} = -(2\pi f_r)^2. \quad (11)$$

Hereby, *R* is the mode based on the resonant frequency f_r. Equation 10 can be rewritten by using this result into:

$$\frac{\partial^4 u(x)}{\partial x^4} - \beta^4 u(x) = 0. \quad (12)$$

After transformation and substitution of the consonants, β^4 concludes in:

$$\beta^4 = \frac{\rho A(2\pi f_r)^2}{EI}. \quad (13)$$

In practice, only $\beta \neq 0$ is relevant. Therefore, the following general solution is formed:

$$u(x) = \alpha_1 \sin(\beta x) + \alpha_2 \cos(\beta x) + \alpha_3 \sinh(\beta x) + \alpha_4 \cosh(\beta x). \quad (14)$$

The coefficients $\alpha_1, \alpha_2, \alpha_3, \alpha_4$ can be determined from the defined boundary conditions. If equation 14 is applied to the boundary conditions of equations 6 to 9, equations 15 to 18 result.

$$u(x)|_{x=0} = 0 = \alpha_2 + \alpha_4 \quad (15)$$

$$\frac{\partial u(x)}{\partial x}|_{x=0} = 0 = \beta(\alpha_1 + \alpha_3). \quad (16)$$

$$\frac{\partial^2 u(x)}{\partial x^2}|_{x=l} = 0 = \beta^2(-\alpha_1 \sin(\beta l) - \alpha_2 \cos(\beta l) + \alpha_3 \sinh(\beta l) + \alpha_4 \cosh(\beta l)) \quad (17)$$

$$\frac{\partial^3 u(x)}{\partial x^3}|_{x=l} = 0 = \beta^3(-\alpha_1 \cos(\beta l) - \alpha_2 \sin(\beta l) + \alpha_3 \cosh(\beta l) + \alpha_4 \sinh(\beta l)) \quad (18)$$

Hereby, l equals the length of the beam. By inserting these boundary conditions into equation 14, the characteristic matrix of matrices *(M)*:

$$\begin{bmatrix} 0 & 1 & 0 & 1 \\ \beta & 0 & \beta & 0 \\ -\beta^2 \sin(\beta l) & -\beta^2 \cos(\beta l) & \beta^2 \sinh(\beta l) & \beta^2 \cosh(\beta l) \\ -\beta^3 \cos(\beta l) & \beta^3 \sin(\beta l) & \beta^3 \cosh(\beta l) & \beta^3 \sinh(\beta l) \end{bmatrix} \begin{bmatrix} \alpha_1 \\ \alpha_2 \\ \alpha_3 \\ \alpha_4 \end{bmatrix} = \begin{bmatrix} 0 \\ 0 \\ 0 \\ 0 \end{bmatrix} \quad (19)$$

The solution for the coefficients is ≠ 0 when the determinant of the matrix is zero. If the determinant corresponds to zero (*det(M) = 0)*, the frequency equation is obtained with the help of trigonometric identities:

$$\cos(\beta l)\cosh(\beta l) = -1 \quad (20)$$

A transcendental equation concludes for the natural frequency and results in the following three values after conversion (Inman, 2013):

$$\beta = \left\{\frac{1.8752}{l}, \frac{4.6941}{l}, \frac{7.8548}{l}\right\} \quad (21)$$

The function $\emptyset_r(x)$ is based on this information:

$$\emptyset_r(x) = \frac{cosh(\beta_r l) - cos(\beta_r l)}{\sinh(\beta_r l) - sin(\beta_r l)}(\sinh(\beta_r x) - \sin((\beta_r x)) - \cosh(\beta_r x) + \cos(\beta_r x) \quad (22)$$

2.2 Simulative modal analysis und harmonic response analysis with ANSYS

Simulative modal analysis using the finite element method (FEM) is a good way to determine the quality of the additive design structure and its dynamic properties. For the FEM, different solution functions are available in ANSYS such as the Reduced Method, the Subspace Method, Unsymmetrical Method and Damped Method. There is also the Block Lanczos Method, which is suitable for undamped linear systems with symmetrical matrices (Lanczos, 1950).

In general, the FEM attributes discretization to the differential equation systems, so that typical structural dynamic problems arise during the solution. Based on the dÁlemberts principle, the generalized equation of motion of the discretization process of a continuous structure can be described with FEM:

$$M\ddot{q} + C\dot{q} + Kq = F(t) \quad (23)$$

Thereby, *M* is the mass matrix, $\ddot{q}$ the second derivative of the displacement *q*, $\dot{q}$ the velocity, *C* the damping matrix, *K* the stiffness matrix and *F(t)* the vector of applied forces at the time *t*. In ANSYS, programmed FEM codes exist for the solution of static displacement and static stresses,

natural frequencies and mode forms, forced harmonic response amplitude and dynamic stress, transient dynamic behavior and transient stresses, so that the first part of the solution for the free oscillation of the structure can be given with the following matrix equation (Rieger, 1986):

$$M\ddot{q} + Kq = 0 \tag{24}$$

With this equation, the natural frequencies and the mode forms of linear undamped systems can be determined and correspond mathematically to the solution of an eigenvalue problem. With modal analysis, the dynamic properties of the model can be understood and based on this, a harmonic response analysis can be performed to determine the behavior of the structure under a stationary sinusoidal (harmonic) load at a certain frequency:

$$F = \left(F_{max}e^{j\psi}\right)e^{j\Omega t} \tag{25}$$

$$q = \left(q_{max}e^{j\theta}\right)e^{j\Omega t} \tag{26}$$

where e^j is the sinusoidal motion with a phase shift and Ω is the excitation frequency at which the load is applied. There may be a force shift ψ due to different loads and a phase shift θ. The answer of harmonic response analysis is then solved with:

$$(-\Omega^2 M + j\Omega C + K)(x_1 + jx_2) = (F_1 + jF_2) \tag{27}$$

3. Background

Deterministic causes of the inherent non-linearity such as material deformations, friction between the tool and workpiece, chip separation and shear chip formation, can lead to self-induced vibrations during machining (Antic et al., 2012). With increasing tool wear, the cutting forces increase, especially for materials that are difficult to machine, so that intensively forced vibrations are added on top of the self-induced vibrations (Gutnichenko et al., 2016). Figure 3 shows the tool vibrations caused by chip formation based on a metrological analysis. The Berger PFS special machine was used for these preliminary investigations. A Kistler 9255 force measurement platform was installed to measure the tool vibrations.

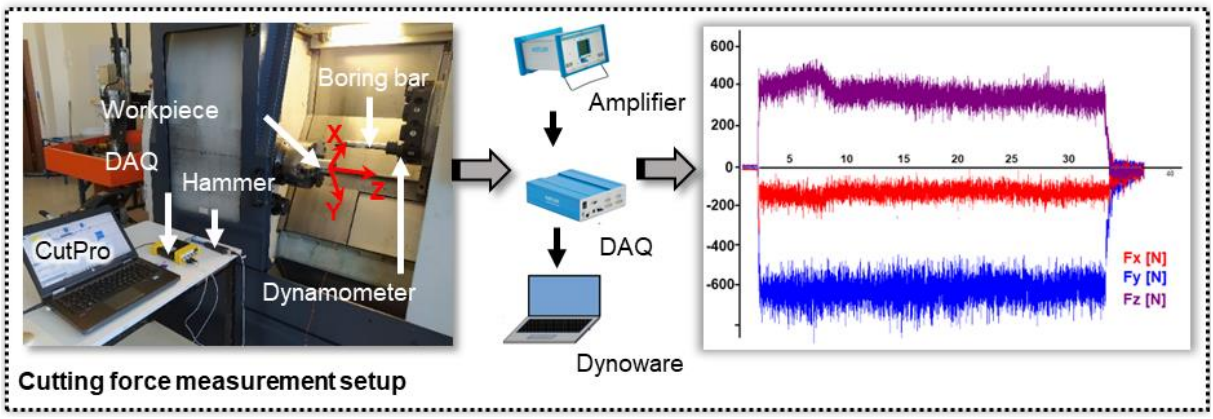

Figure. 3. Tool vibrations caused by segmented chip formation

To improve vibration and damping behavior, additional damping elements could be attached to the tool holder, while passive vibration damping could be possible by modifications inside the tool holder. In order to make very good use of the space inside the tool holder and still guarantee an appropriate stability, a hollow three-dimensional support structure, originating from hexagonal cells which naturally occur in honeycomb structures, was constructed out of truncated octahedrons.

4. Additively manufactured internal structure of a truncated octahedron for vibration damping

The biotonic structure of honeycombs consists of hexagonal cells, is stable, does not deform easily and has excellent compressive and bending strength (Bao et al., 2016). Among other things,

the high elongation and tensile strength is an important feature which is achieved through the uniformity of the honeycomb structure, which is advantageous for the expansion of existing application areas (Iwanaga et.al., 2009). Honeycomb structures are usually used for lightweight and high-strength composite materials, e. g. for the manufacturing of sandwich panels in aerospace technology (Chen et al., 2012). Due to their efficient structure, honeycomb-cored sandwich panels can be used in the railway industry and as high strength reinforcement for high-speed vessels hulls (Rao et al., 2012). The structure of the honeycomb can shift resonance frequencies and improve vibration characteristics by appropriate geometric changes of the repeating unit cells.

Archimedean polyhedral are suitable for spatial structures, since they present a regular symmetry and a good approximation to the spherical surface (Suárez et al., 2008). Besides the tetrahedron, hexahedron, icosahedron and dodecahedron, the octahedron belongs to the regular polyhedral. Mathematically, the basic bodies of the polyhedral are solid bodies bounded by surface polygons (Chieh, 1979). The truncated octahedron is created by joining two square pyramids together at their bases to form an octahedron and then cutting at all six corners by one third of the edge length of each vertex (Weck et al., 2005). The octahedron stump consists of six square and eight hexagonal surfaces, i.e. they are not congruent to each other, so that it is no longer a regular polyhedron (Chieh, 1979). The geometry consists of 24 corners and 36 edges of equal length. The geometry of a hollow octahedron stump was chosen as a support structure, so that the space inside the tool holder could be filled out completely and the vibration properties could be improved. In this way, the advantages of honeycomb structures and the truncated octahedron could be exploited (Figure 4).

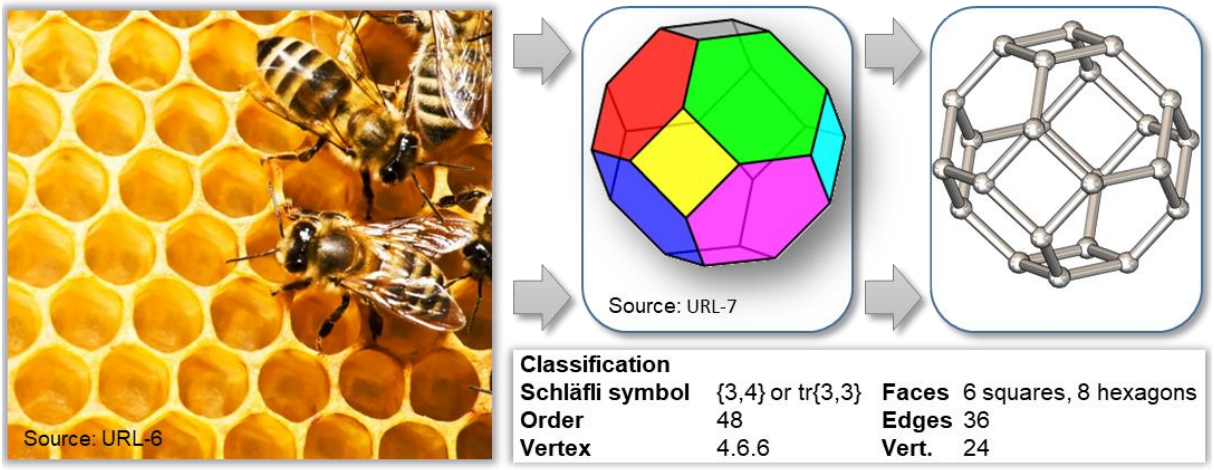

Figure. 4. Combining the advantageous properties of the honeycomb structure and the truncated octahedron into a hollow support structure to reduce the vibrations of the tool holder for turning; Sources (URL-6; 2024; URL-7, 2024)

The main reason for choosing the truncated octahedron shape for the internal support cage in this study is that this structure can fill space without gaps or overlaps, creating a continuous skeleton that can support loads throughout the whole internal space of the tool holder. Truncated octahedron cells provide a more even stress distribution and a high stiffness-to-weight ratio by carrying loads in multiple directions (axial, radial, and diagonal) thanks to their spatial structure consisting of six square and eight hexagonal faces. This, especially when combined with cross-reinforcement elements, helps to reduce vibration by limiting bending and shear deformations.

5. Modelling and simulation

The realization of the three-dimensional CAD modelling, including a possibility to vary the size

and proportions of the truncated octahedron elements as well as the matrix dimensions, was a very challenging task, due to the complex and abstract geometry of the hollow structure. To completely define the chosen octahedral geometry, a mathematical basis had to be created, which could then be used for the construction of the ingenious symmetry structure. On this basis, it was necessary to develop an appropriate software module, since a gapless and overlapping-free matrix structure consisting of several hundred complex truncated octahedron elements, as well as their change in dimensions, would not be possible by means of conventional CAD software.

5.1 Development of a mathematical model to define the truncated octahedron geometry

The corners of the truncated octahedron were defined depending on to its center, to subsequently define the overall structure. Since the octahedron stump consists of two cut off pyramids with a square base area, the height of one of the cut off pyramids is doubled, to obtain the truncated octahedron element height:

$$E = 2\sqrt{2}\,a. \tag{28}$$

A mathematical model was developed to systematically define the three-dimensional hollow geometry of the truncated octahedron. First, the corners of a truncated octahedron centered at the origin $\vec{P}_0 = (x_0 \mid y_0 \mid z_0)$ were defined as the vertex $\vec{P}_i$ in depending on the three coordinate axes x, y and z in the three-dimensional space $\mathbb{R}^3$ (Figure 5 a). The 24 vertices can be described with the following equation depending on the element height E:

$$\vec{P}_i(x,y,z) = \begin{pmatrix} x_0 \\ y_0 \\ z_0 \end{pmatrix} + \begin{pmatrix} x \\ y \\ z \end{pmatrix} \frac{E}{4}, \quad whereby \begin{cases} |x| \neq |y| \neq |z| \in \mathbb{N}^* \\ E \in \mathbb{N}^* \mid E \neq 0 \\ -2 \leq x,y,z \leq 2 \end{cases}. \tag{29}$$

Consequently, using the control variable i, the 24 vertices of the truncated octahedron were subsequently numbered ascending in y-direction and clockwise. This can be illustrated by the projection of a spherical helix, which tangents all vertices starting at $\vec{P}_1$ and increases in width while approaching the geometries center and subsequently decreases in width until reaching the vertex $\vec{P}_{24}$, which is illustrated in Figure 5 b. The 36 edges K_n of the truncated octahedron were defined as a function of the vertices $\vec{P}_i$ and were assigned to the according surfaces, which are illustrated in color Figure 5 c. As illustrated in Figures 5 and 6, the cell geometry employed in the study was defined in this manner for specific reasons. As illustrated in Figure 5, a mathematical structure was devised to ascertain the surface and edge relationships of the truncated octahedron. This structure is imperative for the OctMatrix software to generate the cell matrix without overlap or gaps. Conversely, Figure 6 illustrates the cross-reinforcement elements employed to enhance the rigidity of the cell, along with the geometric reinforcement that constitutes the foundation for the vibration reduction observed in Model D. Consequently, these two figures distinctly elucidate the geometric underpinnings that justify the observed discrepancies between simulation and experimental outcomes.

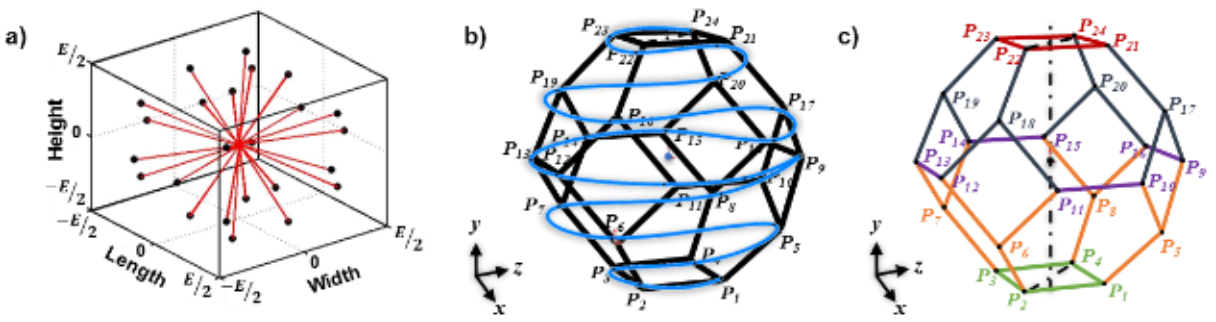

Figure 5. Mathematical description of the truncated octahedron

The resulting linear equations as a function of $\lambda \in [0, 1]$ are colored accordingly. The lower square surface (green) can be described with the following equations:

$$K_n: \vec{s} = \vec{P}_i + \lambda\left(\vec{P}_{i+1} - \vec{P}_i\right) \mid 1 \le i \le 3,\ n = i$$

$$K_n: \vec{s} = \vec{P}_i + \lambda\left(\vec{P}_{i-3} - \vec{P}_i\right) \mid i = 4,\ n = i.$$

As an example, the edge K_1 is described by:

$$K_1: \vec{s} = \begin{pmatrix} x_0 \\ y_0 \\ z_0 \end{pmatrix} + \begin{pmatrix} 1 \\ -2 \\ 0 \end{pmatrix} \frac{4}{E} + \lambda \left[\left(\begin{pmatrix} x_0 \\ y_0 \\ z_0 \end{pmatrix} + \begin{pmatrix} 0 \\ -2 \\ -1 \end{pmatrix} \frac{4}{E}\right) - \left(\begin{pmatrix} x_0 \\ y_0 \\ z_0 \end{pmatrix} + \begin{pmatrix} 1 \\ -2 \\ 0 \end{pmatrix} \frac{4}{E}\right)\right]$$

$$K_1: \vec{s} = \begin{pmatrix} x_0 \\ y_0 \\ z_0 \end{pmatrix} + \begin{pmatrix} 1 \\ -2 \\ 0 \end{pmatrix} \frac{4}{E} + \lambda \left(\begin{pmatrix} -1 \\ 0 \\ -1 \end{pmatrix} \frac{4}{E}\right). \quad (30)$$

Together with the orange and purple marked edges, the edges of the lower square surface (green) form the lower hexagonal surfaces as follows:

$$K_n: \vec{s} = \vec{P}_i + \lambda\left(\vec{P}_{i+4} - \vec{P}_i\right) \mid 1 \le i \le 4,\ n = i + 4$$

$$K_n: \vec{s} = \vec{P}_i + \lambda\left(\vec{P}_{2i-1} - \vec{P}_i\right) \mid 5 \le i \le 8,\ n = 2i - 1$$

$$K_n: \vec{s} = \vec{P}_i + \lambda\left(\vec{P}_{2i} - \vec{P}_i\right) \mid 5 \le i \le 8,\ n = 2i$$

$$K_n: \vec{s} = \vec{P}_{2i} + \lambda\left(\vec{P}_{2i+1} - \vec{P}_{2i}\right) \mid 5 \le i \le 7,\ n = i + 12$$

$$K_n: \vec{s} = \vec{P}_{2i} + \lambda\left(\vec{P}_{i/2+1} - \vec{P}_{2i}\right) \mid i = 8,\ n = i + 12. \quad (31)$$

Originating from the vertices of the middle edges (purple), the edges of the upper hexagonal surfaces are described:

$$K_n: \vec{s} = \vec{P}_{2i-1} + \lambda\left(\vec{P}_{i+12} - \vec{P}_{2i-1}\right) \mid 5 \le i \le 8,\ n = 2i + 11$$

$$K_n: \vec{s} = \vec{P}_{2i} + \lambda\left(\vec{P}_{i+12} - \vec{P}_{2i}\right) \mid 5 \le i \le 8,\ n = 2i + 12$$

$$K_n: \vec{s} = \vec{P}_i + \lambda\left(\vec{P}_{i+4} - \vec{P}_i\right) \mid 17 \le i \le 20,\ n = i + 12. \quad (32)$$

Concluding, the upper square surface is defined:

$$K_n: \vec{s} = \vec{P}_i + \lambda\left(\vec{P}_{i+1} - \vec{P}_i\right) \mid 21 \le i \le 23,\ n = i + 12$$

$$K_n: \vec{s} = \vec{P}_i + \lambda\left(\vec{P}_{i+1} - \vec{P}_i\right) \mid i = 24,\ n = i + 12. \quad (33)$$

With the following equation, the cross strutting was defined, which is visualized in Figure 6. For this purpose, additional 24 edges were created, which connect all vertices $\vec{P}_i$ to the origin $\vec{P}_0 = (x_0 \mid y_0 \mid z_0)$, whereby the condition $\lambda \in [0, 1]$ in turn applies to the resulting linear equations.

$$K_n: \vec{s} = \vec{P}_i + \lambda\left(\vec{P}_0 - \vec{P}_i\right) \mid 1 \le i \le 24,\ n = i + 36 \quad (34)$$

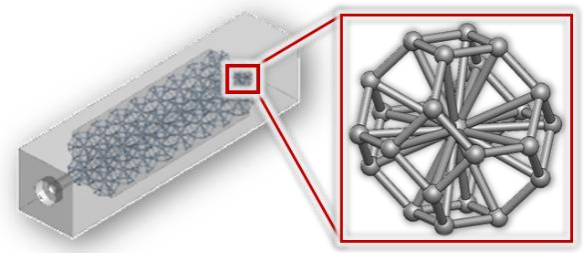

Figure 6. Truncated octahedron with cross strut

5.2 Development of the software module OctMatrix

The construction of the three-dimensional truncated octahedron model is a complex task. To create a tessellation out of truncated octahedrons, referred to as building blocks, it is necessary to connect them via a transitional phase or matrix. To simplify this task and to be able to create various tessellations to seamlessly fill the tool receiver, according to algorithms and a suitable user interface were programmed and designed in the VBA environment of the construction software SolidWorks, originating from the mathematical formulations above. Thereby, single building blocks are systematically connected while avoiding the overlapping of constructional elements to prevent resulting inconsistencies. The designed graphical user interface (GUI) is presented in Figure 7, while an according flow chart describing the programmed procedures is shown in Figure 8. Prior to starting the developed software module, the construction software SolidWorks needs to be initialized, since all according calculations and the CAD design are

carried out within. After initializing the software module OctMatrix, the user is asked to provide a user path and chooses the element size for a single truncated octahedron. Necessary input parameters for the construction of the building block matrix are the number of elements in x-, y-, and z-direction, while the number of elements in y- and z-direction must be equal, to ensure a fitting and symmetrical fill geometry for the tool holder. Choices for cross strutting and pyramidal matrix edges can be made by the user, who also chooses the diameters for the tube profile and edge spheres.

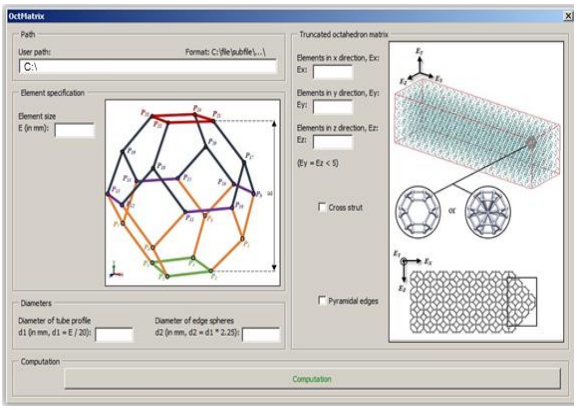

Figure 7. GUI of OctMatrix

The algorithms developed for the software module OctMatrix are based on the mathematical equations presented in section 4.1 and are presented in Figure 9. On the left side, the construction of a single building block with the option of cross strutting is illustrated in a simplified approximation, while the main function to create the matrix including the query for pyramidal edges is shown on the right side.

The OctMatrix module automatically checks that the cells are geometrically correct in a few steps after creating the cage structure parametrically. First, the system checks for problems with how cells are arranged. If there are any problems, the cells are rearranged. In the last stage, the model is moved to the CAD/FEA environment, and an extra check is done for situations that do not meet the watertight solid condition during mesh generation.

5.3 Designed additive matrix-structures

Figure 10 shows the four different tool holders, which were designed with OctMatrix and afterwards evaluated by investigating the passive damping of process vibrations. The standard tool holder in its conventional massive form (type A) was used as a reference model. The inner structures of the further developed models were designed with the created software module OctMatrix. Thereby, the building blocks in form of truncated octahedrons were arranged in different variations and element sizes. The inner structure designed for the tool holder type B consists of smaller elements than type C or D arranged in a 16x4x4 matrix. Unlike type C, type D consists of building blocks with cross strutting, while both structures were arranged in an 8x2x2 matrix.

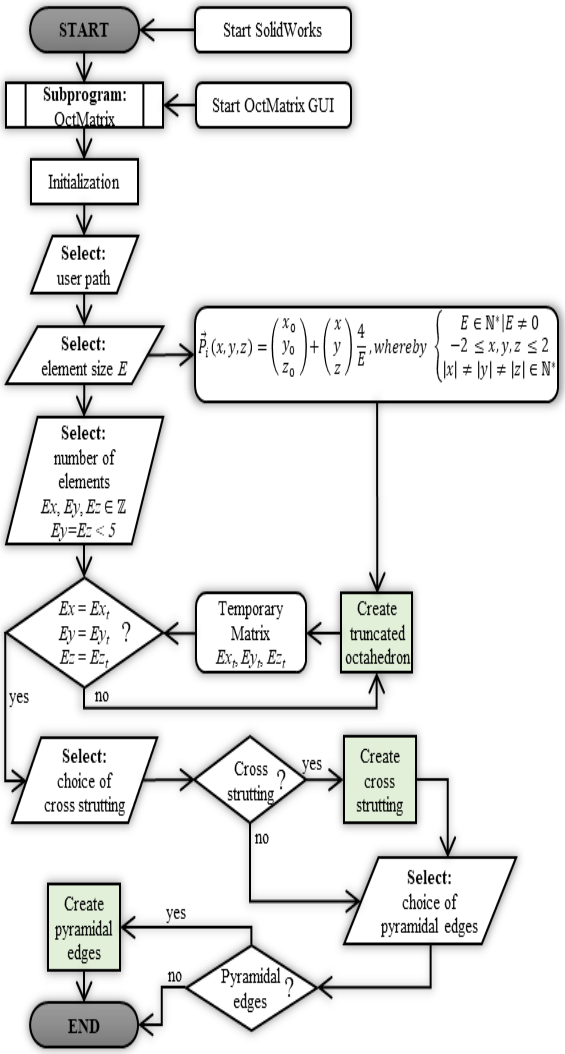

Figure 8. Flow chart of OctMatrix

Create Truncated Octahedron(x, y, z)
Draw a point cloud describing the corners of a truncated octahedron (specified by eq. 1 and eq. 2) with the element size E declared by user, centered at the input coordinates (x, y, z)
  for each point P_i **do**
    Create a sphere centered at P_i with the diameter d_1 declared by user
end for
for each pair of points P_j and P_k (specified by eq. 3–6) **do**
  Draw a line between P_j and P_k
  Create a tube profile with the diameter d_2 declared by user enclosing the line
end for
%% Choose cross strutting **%%**
if user chose cross strutting **do**
  Create a sphere centered at the input coordinates (x, y, z) with the diameter $d_1 \cdot 2$
  for each pair of points P_i and P_0 (specified by eq. 7) **do**
    Draw a line between P_i and P_0
    Create a tube profile with the diameter d_2 declared by user enclosing the line
  end for
end if

Create Matrix(Ex, Ey, Ez)
counter $i_x = 0$
for number of elements in x-direction (E_x-1) **do**
  counter $i_y = 0$
  counter $i_z = 0$
  for number of elements in y-direction (E_y-1) **do**
    for number of elements in z-direction (E_z-1) **do**
      Create Truncated Octahedron($E \cdot i_x, E \cdot i_y, E \cdot i_z$)
      $i_z = i_z + 1$
    end for
    $i_y = i_y + 1$
  end for
  $i_x = i_x + 1$
end for
%% Choose pyramidal edges **%%**
if user chose pyramidal edges **do**
  counter $i_{Edge} = E_y$-1
  while $i_{Edge} > 0$ **do**
    Add an $i_{Edge} \cdot i_{Edge}$ grid of truncated octahedrons on both sides of the matrix
    $i_{Edge} = i_{Edge}$-1
  end while
end if

Figure 9. Descriptive algorithms for OctMatrix

6. Vibration simulation

The vibration simulation of the tool holders was carried out via modal analysis and frequency response analysis. Modal analysis is used to determine the natural frequencies and natural oscillations whereas the frequency response analysis is used to calculate the structure's response to harmonic and time variable loads.

6.1 Modal analysis

In the modal analysis, the structural dynamics of tool holders A to D were investigated. In order to determine the vibration forms, no excitations or loads (non-linear changes or influences) were taken into account, but the model properties of the respective additive structures by which the tool holders were constructed were investigated. The modal analysis also provided the basis for the following frequency response analysis. Originating from the reference tool, all additively designed support structures were considered in the idealization and discretization by means of FEM. Therefore, the clamping lengths of the tool holders and the material properties of X3NiCoMoTi18-9-5 were defined. During the calculation model preparation, a discretization was carried out, which required special attention due to the additive structures, since the local fineness of the mesh network has an impact on the accuracy of the results (Figure 11).

Type	Truncated Octahedron (TOCT)	Truncated octahedron matrix	Truncated octahedron matrix with pyramidal edges	Tool holder	Characteristics
A	...	...	...	95 mm, A-A, (16x16)mm	Solid model
B	4 mm	4x, 4x, 16x	71.60 mm	95 mm, A-A, (16x16)mm	TOCT matrix = 256 TOCT edges = 28 Total = 284 Outter spheres = 3840 Connecting rods = 7104
C	8 mm	2x, 2x, 8x	71.60 mm	95 mm, A-A, (16x16)mm	TOCT matrix = 32 TOCT edges = 2 Total = 34 Outter spheres = 544 Connecting rods = 944
D	8 mm	2x, 2x, 8x	71.60 mm	95 mm, A-A, (16x16)mm	TOCT matrix = 32 TOCT edges = 2 Total = 34 Outter spheres = 544 Inner spheres = 34 Cross struc = 816 Connecting rods = 1760

Figure 10. Modelled CAD tool holders

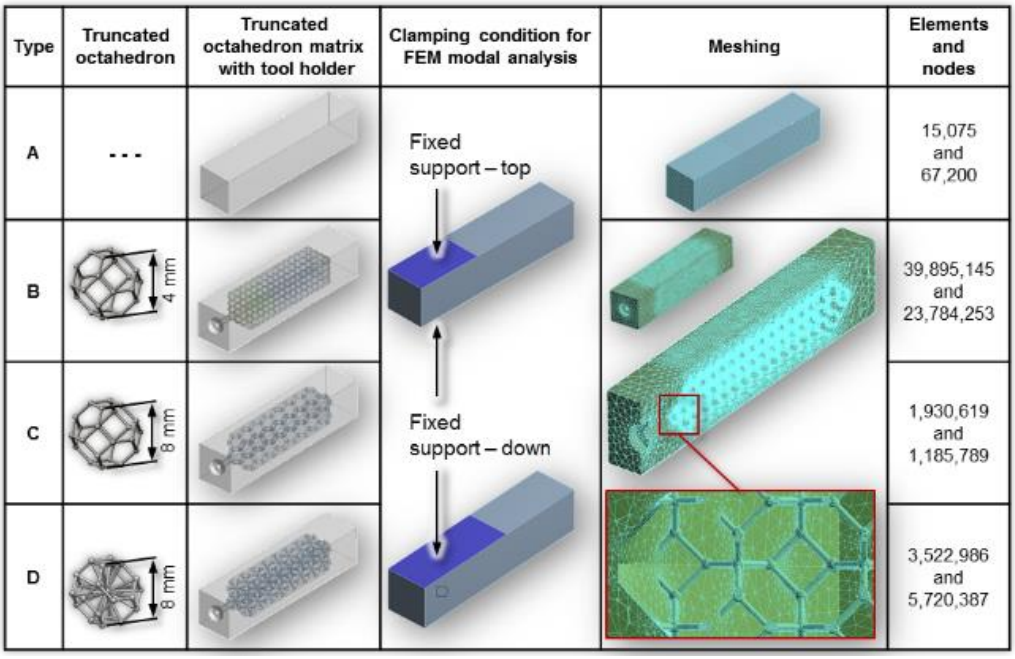

Figure 31. Idealization of the FEM models

The modal analysis resulted in five rigid body eigenmodes for each tool holder, which are displayed in Figure 12. It is clearly visible that the according frequencies are higher for the reference tool holder than for the modified tool holders. The different designed tool holders show similar frequencies. Slightly different eigenmodes are recognizable in Mode 4 and Mode 5 of tool holder D.

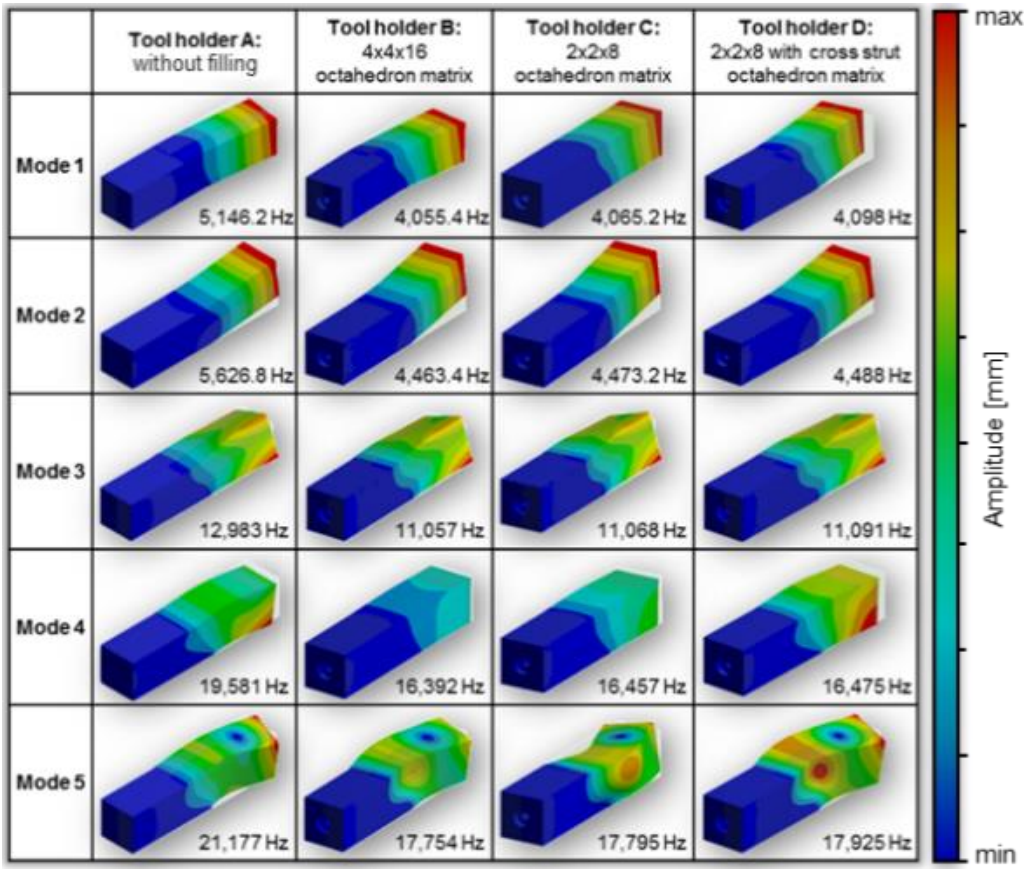

Figure 42. Modes of the tool holder models

6.2 Harmonic response analysis

Based on modal analysis and experimentally determined loads, a harmonic response analysis was performed. In this way, the forced oscillation states of the linear structures were calculated (Figure 13). The aim was to investigate the behavior of additive structures in comparison to the reference model in the form of harmonic frequencies.

7. Experimental investigation/material and methods

Subsequent to the manufacturing of the tool holders, experimental tests were carried out on the CNC lathe. The material X3NiCoMoTi18-9-5, whose chemical composition is listed in Table 1, was processed. A hammer measurement was then carried out. The tool holders were positioned in the clamping lengths as usual during turning and stimulated with the impulse hammer method to determine the dynamic behavior of the respective structures. A force sensor located on top of the impulse hammer hit the outer edge of the tool holder, during the force contact was measured with an acceleration sensor (Figure 14). Prior to the experiments, both the force sensor and the accelerometer were calibrated by the manufacturer and verified in-house using a reference calibration signal in accordance with ISO 16063-21. The impulse hammer was checked using the built-in electronic calibration function, while the accelerometer sensitivity was verified with a 1g reference excitation. All devices were within the specified calibration periods, and no deviations outside the allowable tolerances were detected. Therefore, the measurement results presented in this study are based on fully calibrated and traceable instrumentation.

The present study is founded upon the vibration damping mechanism, the energy distribution within the structure, and the passive damping principles arising from internal friction. During harmonic response analysis, the damping coefficient, denoted by $\zeta = 0.022$, was calculated using the modal logarithmic decrement method, which is based on the complex modal parameters of the structure.

The internal lattice structure, particularly due to the multidirectional load transfer of truncated octahedron cells and the increased diagonal stiffness with cross struts, causes the vibration energy to spread over a larger volume and generates more internal friction between the elements. This contributes to an increase in the equivalent damping ratio of the structure and a significant decrease in peak resonance amplitudes. The passive damping technique is predicated on micro-scale friction and local energy losses that occur during elastic deformation in the strut-node regions within the cage. In particular, the cross struts employed in Model D have been shown to increase shear deformations, thereby enhancing the structure's hysteretic damping capacity and leading to a greater damping of the resonance peaks observed in the experimental FRF curves.

In this study, the vibration behavior of the four tool holder configurations (A–D) was evaluated through a controlled experimental setup designed to ensure repeatability and comparability of the results.

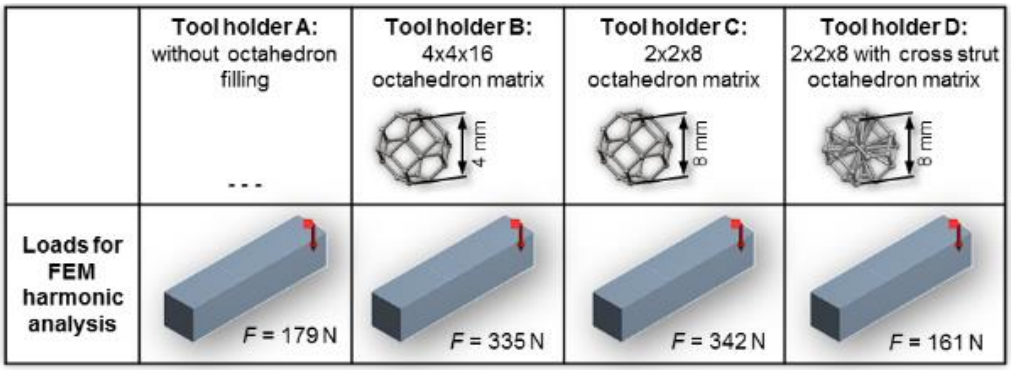

Figure 53. Simulation setup for the harmonic response analysis

Each tool holder was mounted with an identical clamping length of 195 mm, and the same X3NiCoMoTi18-9-5 workpiece material was used in all trials. The excitation was applied using an instrumented impulse hammer at the same location on the free overhanging end of the tool holder to generate repeatable broadband dynamic input. An ICP-type accelerometer was positioned at the same measurement point on each tool holder to capture the vibration response. For each configuration, three repeated impact tests were performed, and the averaged Frequency Response Function (FRF) was used to minimize random variations. This approach ensured that all tool holders were evaluated under identical boundary conditions, providing a consistent basis for comparing the effects of the internal lattice structures.

Table 1. Chemical composition of alloy tool steel X3NiCoMoTi18-9-5 (wt.-%)

	Ni	Co	Mo	Ti	Al	Cr	Cu	C	Mn	Sn	P	S
1.2709	17-19	8.5-9.5	4.5-5.2	0.11	0.05-0.15	≤0.5	≤0.5	≤0.03	≤0.1	≤0.1	≤0.01	≤0.01

Note: Reproduced from Sehrt etal. (2017)

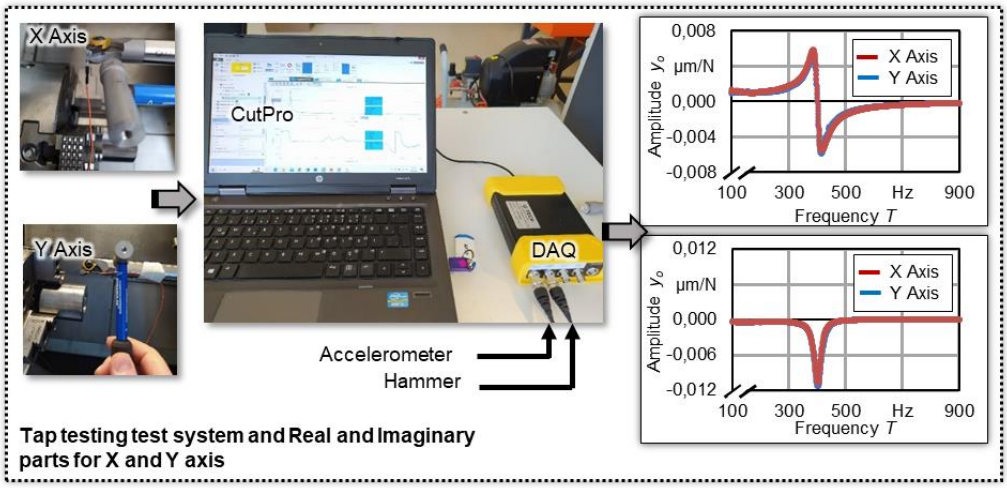

Figure 64. Experimental setup

To validate the experimental modal characteristics and to support the harmonic response analysis, the CutPro machining dynamics software (developed by Manufacturing Automation Laboratories, University of British Columbia) was used. CutPro is a specialized industry-standard tool for predicting machining stability, chatter vibrations, modal behavior, and frequency response functions of tool–holder–spindle systems. In this study, the experimentally obtained modal parameters were imported into CutPro in order to generate reference stability maps and to verify the consistency of the harmonic response trends observed in ANSYS simulations.

8. Results

Figure 14 shows the results of the harmonic response analysis and the experiments in relation to the amplitude of the respective frequency. The high amplitude deflection of the tool holder B is remarkable, which can be attributed to the small 3D truncated octahedron models and the resulting matrix-cell structure of 4x4x16. As demonstrated in Figure 15, an analysis of the frequency-amplitude curves indicates that the most effective parameters for vibration reduction are the strut connection density and the element size of the internal cage geometry. Specifically, the cross-strut structure applied in Model D increases both axial and diagonal stiffness in comparison with Model C, which has the same number of cells. This results in a reduction in the amplitude of harmonic excitations by approximately 50%.

Furthermore, a reduction in the cell element size (Ex, Ey, Ez) (Model B) has been observed to increase the load per strut, resulting in structural imbalance and an increase in the resonance amplitude. The findings presented in Figure 14 demonstrate that the most effective parameters in vibration reduction are 'cross-brace usage', 'cell size', and 'matrix arrangement'. This suggests that the optimal design is a cage structure with a low number of cells but high connection density.

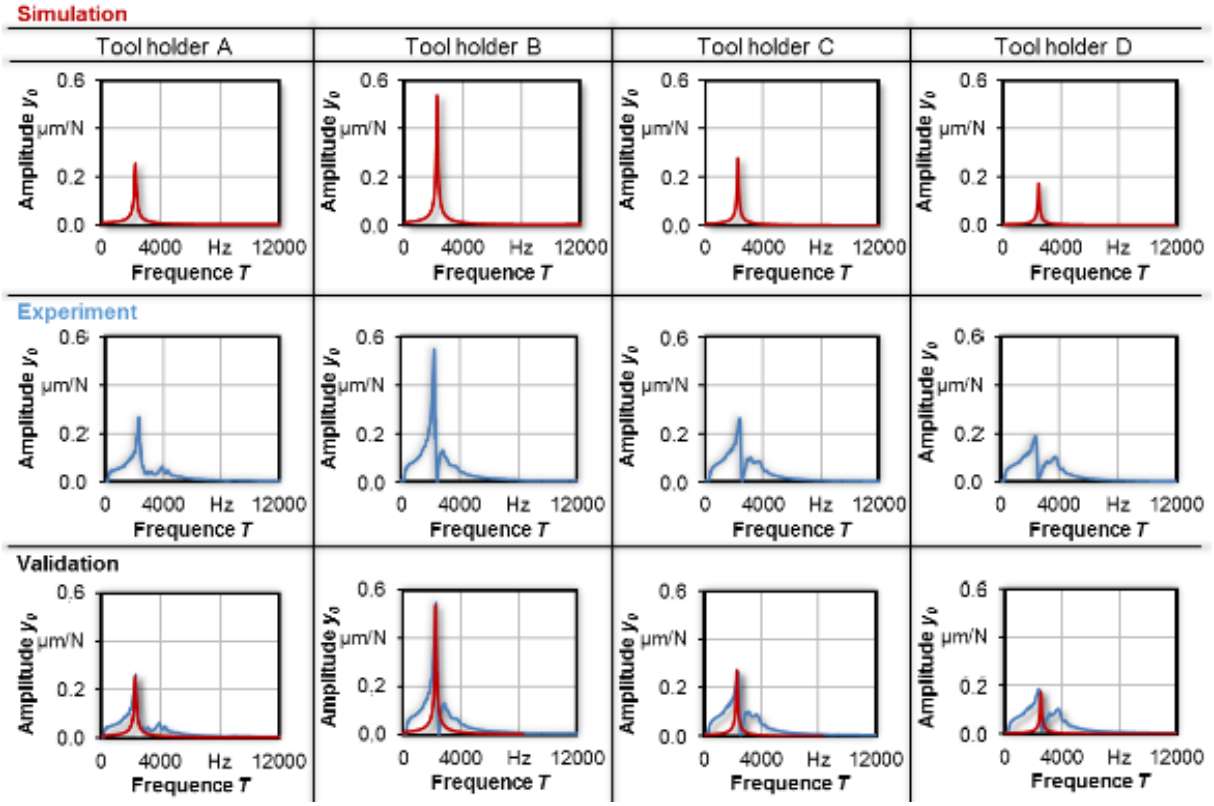

Figure 75. Comparison of the experimental and simulative vibration forms of the tool holders

Table 2 shows an overview of the simulatively examined tool holders. Based on the mathematical model and the programming of the OctMatrix software module, the different matrix-cell structures could be constructed and implemented inside the tool holder. The software parameters and according to matrix structure resulted in varying computing times for the CAD structure creation, as well as the number of networking elements and nodes for the simulation. The resulting values for the total deformation and the reference stress in the tool holder D are clearly below those of the other tool holders and could be reduced significantly compared to the reference model, concluding in an effective vibration damping.

9. Conclusion

This paper presents the development of a mathematical model for the construction of three-dimensional support structures designed with truncated octahedron cells and the programming of a suitable software module called OctMatrix for the construction of variable matrix-cell structures. The aim of this investigation was to reduce the vibrations of a tool holder used for turning, by implementing an internal supporting matrix structure with the additive SLM process. Three different matrix-cell structures were constructed inside the tool holder. The eigenforms and eigenfrequencies were analyzed using a simulative modal analysis and harmonic response analysis. The data of the individual loads for the tool holders could be determined experimentally after prototype production and used for a harmonic response analysis. The results showed

that the implementation of the matrix-cell structure with 2x2x8 truncated octahedron elements with cross strut leads to a significant improvement compared to the reference tool holder model. The total deformation could be reduced by approx. 90 % and the reference stress by approx. 18 %, which resulted in an effective vibration damping of the tool holder.

In this study, dimensional tolerances specific to the SLM process and geometric deviations that may occur in thin-walled regions have not been considered. It is imperative to address the discrepancies between the geometry produced in the experimental study and the designed geometry, along with the potential consequences of these discrepancies.

Table 2. Overview of the simulated examinations carried out

	Tool holder A	**Tool holder B**	**Tool holder C**	**Tool holder D**
Software module: OctMatrix parameter	–	$E_x = 16$, $E_y = 4$, $E_z = 4$	$E_x = 8$, $E_y = 2$, $E_z = 2$	$E_x = 8$, $E_y = 2$, $E_z = 2$ with cross strut
Solver time of OctMatrix	–	12 h	5 h	8 h
Harmonic analysis				
Impulse hammer force	179 N	335 N	342 N	161 N
Meshing				
Elements	15,075	39,895,145	1,930,619	3,522,986
Nodes	67,200	23,784,253	1,185,789	5,720,387
Modal analysis				
Mode 1	5,146.2 Hz	4,055.4 Hz	4,065.2 Hz	4,098 Hz
Mode 2	5,626.8 Hz	4,463.4 Hz	4,473.2 Hz	4,488 Hz
Mode 3	12,983 Hz	11,057 Hz	11,068 Hz	11,091 Hz
Mode 4	19,581 Hz	16,392 Hz	16,457 Hz	16,475 Hz
Mode 5	21,177 Hz	17,754 Hz	17,795 Hz	17,925 Hz
Results				
Total deformation	0.0445 mm	0.1349 mm	0.0097 mm	0.0045mm
Reduced vibration	Reference model	303.2 %	-78.3 %	-98.7 %
Equivalent stress	32.195 MPa	77.599 MPa	66.095 MPa	26.454 MPa

Acknowledgments

I would like to thank the Department of Mechanical Engineering at Recep Tayyip Erdoğan University's Faculty of Engineering for their support in conducting the research conducted for this study. I would also like to thank all the research assistants and technical staff who contributed to the provision of laboratory facilities and the preparation of test equipment during the experimental study.

Financing Statement

This research has not received any specific grant from any funding organization, commercial or non-profit sector.

Conflict of Interest Statement

The authors declare that they have no conflict of interest.

Ethical Standards

No Ethics Committee Approval is required for this study

References

Abdarrhim, M.A. (2021). Euler-Bernoulli and timoshenko beam theories analytical and numerical comprehensive revision. *European Journal of Engineering and Technology Research*, 6(7), 20–32. https://doi.org/10.24018/ejeng.2021.6.7.2626.

Aggogeri, F., Borboni, A., Merlo, A., Pellegrini, N., Ricatto, R. (2017). Vibration damping analysis of lightweight structures in machine tools. *Materials*, 10(3), 2–14. https://doi.org/10.3390/ma10030297

Akesson, H. (2007). Active control of vibration and analysis of dynamic properties concering machine tools, Dissertation, Blekinge Institute of Technology, Sweden.

Antic, A., Zeljkovic, M., Petrovic, P.B., Zivkovic, A., Hodolic, J. (2012). Experimental analysis and fem modelling of a cutting tool vibrations. *Strojarstvo*, 54(2), 117–125.

Astakhov, V.P.and Quteiro, J.C. (2008). Tools (geometry and material) and tool wear. In: *Machining: fundamentals and recent advances* (Eds. Davim, J.P.), Springer, ISBN: 978-1-848-00213-5, London, England. https://doi.org/10.1007/978-1-84800-213-5

Bao, N., Ma, J., Zahng, X., Zhong, Z. (2016). Structural bionic lightweight design for the stiffened plate of base structure, *7th International Conference on Mechanical and Aerospace Engineering (ICMAE)*, 2016, London, United Kingdom.

Bikas, H., Stavropoulos, P., Chryssolouris, G. (2016). Additive manufacturing methods and modelling approaches: a critical review. *The International Journal of Advanced Manufacturing Technology*, 83(1-4), 389–405. https://doi.org/10.1007/s00170-015-7576-2

Cacace, S., Demir, A.G., Semeraro, Q. (2017). Densification mechanism for different types of stainless steel powders in selective laser melting. *Procedia CIRP*, 62, 475–480. https://doi.org/10.1016/j.procir.2016.06.010

Calignano, F., Manfredi, D., Ambosio, E.P., Biamino, S., Lombardi, M., Atzeni, E., Salmi, A., Minetola, P., Luliano, L., Fino, P. (2017). Overview on additive manufacturing technologies. *Proceedings of the IEE*, 105(4), 593–612. https://doi.org/10.1109/JPROC.2016.2625098

Chen, J.X., Gu, C.L., Wan, C.F., Xie, J., Hu, X.Q., Guo, S.J. (2012). Development of integrated bionic honeycomb plates. *Advanced Materials Research*, 450-451, 817–821. https://doi.org/10.4028/www.scientific.net/AMR.450-451.817

Chieh, C. (1979). The Archimedean truncated octahedron, and packing of geometric units in cubic crystal structures. *Acta Crystallographica Section A*, 35(6), 946–952. https://doi.org/10.1107/S0567739479002114

Dolph, C.L. (1954). On the timoshenko theory of transverse beam vibrations. *Quarterly of Applied Mathematics*, 12(2), 175–187.

Gibson, I., Rosen, D., Stucker, B., Kohrasani, M. (2021). Additive manufacturing technologies, Springer Cham, , ISBN: 978-3-030-56129-1, Switzerland. 23–51. https://doi.org/10.1007/978-3-030-56127-7

Guessasma, S., Zhang, W., Zhu, J., Belhabib, S., Nouri, H. (2015). Challenges of additive manufacturing technologies from an optimisation perspective. *International Journal for Simulation and Multidisciplinary Design Optimization*, 6(4):A9, 1–13. https://doi.org/10.1051/smdo/2016001

Gutnichenko, O., Bushlya, V., Zhou, J. M., Stahl, J.E. (2016). Tool wear and vibrations generated when turning high-chromium white cast iron with pcbn tools. *Procedia CIRP*, 46, 285–289. https://doi.org/10.1016/j.procir.2016.04.005

Han, S. M., Benaroya, H., Wei, T. (1999). Dynamics of transversely vibrating beams using dynamics of transversely vibrating beams using four engineering theories. *Journal of Sound and Vibration*, 225(5), 935–988. https://doi.org/10.1006/jsvi.1999.2257

Huang, T.C. (1961). The effect of rotatory inertia and of shear deformation on the frequency and normal mode equations of uniform beams with simple end conditions. *Journal of Applied Mechanics*, 28(4), 579–584. https://doi.org/10.1115/1.3641787

Inman, D.J. (2013). Engineering vibration (5. Edition), *Pearson*, ISBN: 978-0-132-28173-7, London, England, 511.

Iwanaga, H., Shiratsuchi, K., Yamazaki, H. (2009). Fabrication and application of honeycomb film. *Fujifilm Research & Development*, 54, 43–47. https://doi.org/10.1016/j.eurpolymj.2017.06.025

Jared, B.H.; Aguilo, M.A.; Beghini, L.L.; Boyce, B.L., Brett, W.C., Cook, A., Kaehr, B. J., Robins, J. (2017). Additive manufacturing. *Scripta Materialia*, 135, 141-147. https://doi.org/10.1016/j.scriptamat.2017.02.029

Lanczos, C. (1950). An iteration method for the solution of the eigenvalue problem of linear differential and integral operators. *Journal of Research of the National Bureau of Standards*, 45(4), 255–282. https://doi.org/10.6028/jres.045.026

Li, Q., Kucukkoc, I., Zhang, D.Z. (2017). Production planning in additive manufacturing and 3D printing. *Computers & Operations Research*, 83, 157–172. https://doi.org/10.1016/j.cor.2017.01.013

Mellor, S.; Hao, L.; Zhang, D. (2014). Additive manufacturing a framework for implementation. *International Journal of Production Economics*, 149, 194–201. https://doi.org/10.1016/j.ijpe.2013.07.008

Pettersson, L. (2002). Vibrations in metal cutting: measurement, analysis and reduction, Dissertation, Blekinge Institute of Technology, Sweden.

Prasad, B. S. and Babu, M. P. (2017). Correlation between vibration amplitude and tool wear in turning: nnumerical and experimental analysis. *Engineering Science and Technology, an International Journal*, 20(1), 197–211. https://doi.org/10.1016/j.jestch.2016.06.011

Rao, K.K., Rao, K.J., Sarwade, A.G., Chandra, M.S. (2012). Strength analysis on honeycomb sandwich panels of different materials. *International Journal of Engineering Research and Application*, 2(3), Pages 365–374.

Rieger, N.F. (1986). The relationship between finite element analysis and modal analysis. *Sound Vibration*, 20, 16.

Robbins, J.; Owen, S.J.; Clark, B.W.; Voth, T.E. (2012). An efficient and scalable approach for generating topologically optimized cellular structures for additive manufacturing. *Additive Manufacturing*, 12, 296–304. https://doi.org/10.1016/j.addma.2016.06.013

Sames, W.J., List, F.A., Pannala, S., Dehoff, R.R., Babu, S. (2016). The metallurgy and processing science of metal additive manufacturing. *International Materials Reviews*, 61(5), 315–360. https://doi.org/10.1080/09506608.2015.1116649

Santos, E.C., Shiomi, M., Osakada, K., Laoui, T. (2006). Rapid manufacturing of metal components by laser forming. *International Journal of Machine Tools and Manufacture*, 46(12-13), 1459–1468. https://doi.org/10.1016/j.ijmachtools.2005.09.005

Sehrt, J.T., Kleszczynski, S., Notthoff, C. (2017). Nanoparticle improved metal materials for additive manufacturing. *Progress in Additive Manufacturing*, 2(4), 179–191. https://doi.org/10.1007/s40964-017-0028-9

Smirnova, T. (2010). Analysis, modeling and simulation of machine tool parts dynamics for active control of tool vibration, Dissertation, Blekinge Institute of Technology, Sweden.

Strano, G.; Hao, L.; Everson, R.M.; Evans, K.E. (2013). A new approach to the design and optimisation of support structures in additive manufacturing. *International Journal of Advanced Manufacturing Techology*, 66 (9-12), 1247-1254. https://doi.org/10.1007/s00170-012-4403-x

Suárez, J.; Gancedo, E.; Álvarez, J.M.; Morán, A. (2008). Optimum compactness structures derived from the regular octahedron. *Engineering Structures*, 30 (11), 3396-3398. https://doi.org/10.1016/j.engstruct.2008.04.030

Sufiiarov, V.S.; Popovich, A.A.; Borisov, E.V.; Polozov, I.A., Masaylo, D.V., Orlov, A.V. (2017). The effect of layer thickness at selective laser melting. *Procedia Engineering*, 174, 126-134. https://doi.org/10.1016/j.proeng.2017.01.179

Thompson, I. and Brougham, R.I. (2018). A direct method for bloch wave excitation by scattering at the edge of a lattice. *The Quarterly Journal of Mechanics and Applied Mathematics*, 71 (1), 1-24. https://doi.org/10.1093/qjmam/hbx022

Timoshenko, S. (1983). History of dtrength of materials, *Dover Publications*, ISBN: 978-0-486-61187-7, New York, America. 141-144

Timoshenko, S.; Gere, J.M. (2012). Theory of elastic stability, *Courier Corporation*, ISBN: 978-0-486-13480-2, New York, America. 1-37

Timoshenko, S. (1921). LXVI. On the correction for shear of the differential equation for transverse vibrations of prismatic bars. *The London, Edinburgh, and Dublin Philosophical Magazine and Journal of Science*, 41(245), 744–746. https://doi.org/10.1080/14786442108636264

Uhlmann, E., Bergmann, A., Gridin, W. (2015). Investigation on additive manufacturing of

tungsten carbide-cobalt by selective laser melting. *Procedia CIRP*, 35, 8–15. https://doi.org/10.1016/j.procir.2015.08.060

URL-1, (2025). https://www.airliquide.com/industry, 20. September 2025.

URL-2, (2024). http://www.airbus.com/, 20. September 2025.

URL-3, (2025). https://www.geaviation.com/, 25. September 2025.

URL-4, (2024). https://www.pankl.com/de/, 28. September 2025.

URL-5, (2024). http://paulscottinfo.ipage.com/, 23. September 2025.

URL-6, (2024). http://blog.ratioform.de/, 23. September 2025.

URL-7, (2024). http://solar-magazine.com/, 26. September 2025.

Vaidya, R. and Anand, S. (2016). Optimum support structure generation for additive manufacturing using unit cell structures and support removal constraint. *Procedia Manufacturing*, 5, 1043–1059. https://doi.org/10.1016/j.promfg.2016.08.072

Vayre, B., Vignat, F., Villeneuve, F. (2012). Designing for additive manufacturing. *Procedia CIRP*, 3, 632–637. https://doi.org/10.1016/j.procir.2012.07.108

VDI 3405 (2014). *Additive manufacturing: basics, definitions, processes*. VDI-Gesellschaft Produktion und Logistik, Germany.

Weaver, W., Timoshenko, S.P., Young, D.H. (1991). Vibration problems in engineering, John Wiley & Sons, ISBN: 978-8-126-54079-2, India. 1-495.

Weck, O.L.; Nadir, W.D.; Wong, J.G.; Bounova, G.; Coffee, T.M. (2005). Modular structures for manned space exploration: the truncated octahedron as a building block, *1st Space Exploration Conference: Continuing the Voyage of Discovery*, 30 January - 1 February 2005, Orlando, Florida.

Wong, K.V. and Hernandez, A. (2012). A review of additive manufacturing. *ISRN Mechanical Engineering*, 2012(4), 1–10. https://doi.org/10.5402/2012/208760